Reappraisal of the work hardening behavior of bulk amorphous matrix composites

Chang-Myeon Lee[a], Kyoung-Won Park[a], Jae-Hoon Lee[b], Hong-Gie Lee[c], Jae-Il Jang[d], Jae-Chul Lee[a],*

[a] Department of Materials Science and Engineering, Korea University, Anam, Seoul 136-701, Republic of Korea
[b] Advanced Materials Division, Korea Institute of Industrial Technology, Incheon 406-840, Republic of Korea
[c] Korea Institute of Industrial Technology, Nano-surface Technology Team, Incheon 404-254, Republic of Korea
[d] Division of Materials Science and Engineering, Hanyang University, Seoul 133-791, Republic of Korea

ARTICLE INFO

ABSTRACT

This paper investigates the origin of work hardening in amorphous composites by directly measuring the hardness variations of crystalline particles and amorphous matrices at various strains. The work hardening of the amorphous composites was caused predominantly by hardening of the amorphous matrices, rather than of the crystalline particles. The hardening mechanism was explained based on the kinetics and thermodynamics.

1. Introduction

In addition to dramatically enhanced plasticity, bulk amorphous composites exhibit a work hardening-like behavior during plastic flow. Considering that most strengthening mechanisms operative in metallic materials are associated with dislocations, the hardening behaviors observed in amorphous composites, where dislocations do not exist, have been regarded as an experimental artifact caused by ignorance of changes in cross-sectional area during uniaxial compression. Recent experimental works demonstrated that amorphous composites exhibited work hardening even when plotted in a true stress–strain curve, suggesting that the work hardening observed from amorphous alloys is an inherent characteristic. Even with clear evidence confirming the existence of work hardening in amorphous composites, the underlying principles causing work hardening in amorphous composites remain disputed, as summarized in Table 1 [1–10].

According to the various interpretations shown in Table 1 to explain the hardening behavior, the origin of the work hardening of amorphous matrix composites can be classified as the hardening caused by either crystalline particles or amorphous matrices. Hufnagel and co-workers [11], Sun et al. [4] and Hays et al. [8] claimed that the work hardening of amorphous composites originates from the plastic deformation of crystalline particles. Given that the strength and volume fraction of crystalline particles are much smaller than those of the amorphous matrix, their claim that the work hardening arises from crystalline particles alone is not sufficient to support the observed strength increment, which usually comprises several hundred MPa.

Careful observation of the recent work by Park et al. [12] implicitly suggests that work hardening can take place even in monolithic amorphous alloys, as further confirmed by Yang et al. [13]. These experimental results support the hypothesis that the work hardening in amorphous composites may arise from the work hardening of amorphous matrices. Eckert et al. [14] reported that the work hardening of amorphous phases stems from the interaction of shear bands, which in turn disturbs their propagation, thereby hardening the alloys. However, as the strength of the shear band is lower than that of the undeformed regions due to the softening associated with shear-induced dilatation (structural disordering) [15], this claimed mechanism may not be appropriate to explain the observed hardening behavior. Therefore, clarification of this longstanding and uncovered problem on the origin of the work hardening is of fundamental significance.

In this study, we discuss the origin of work hardening in amorphous composites by experimentally demonstrating which phases are responsible for the hardening. For this purpose, we prepared two different families of amorphous composites reinforced with crystalline particles having different morphologies, sizes and volume fractions. The hardening behaviors of the amorphous and

* Corresponding author. Tel.: +82 2 3290 3283.
  E-mail address: jclee001@korea.ac.kr (J.-C. Lee).

Table 1
Various mechanical properties and underling mechanisms for the work hardening of amorphous composites.

Composition	σ_y (MPa)	σ_{ult} (MPa)	ε_p (%)	$\Delta\sigma$ (MPa)	Mechanism	Ref.
$Cu_{50}Zr_{30}Ti_{10}Nb_{10}$	1770	2000	2.3	230	N/C	[1]
$(Zr_{0.7}Ni_{0.1}Cu_{0.2})_{82}Ta_8Al_{10}$	1740	2020	8.0	480	N/C	[2]
$(Cu_{0.6}Hf_{0.25}Ti_{0.15})_{90}Nb_{10}$	2160	2625	12.5	465	N/C	[3]
$Zr_{56.2}Ti_{13.8}Nb_{5.0}Cu_{6.9}Ni_{5.6}Be_{12}$	1500	1750	12.0	250	N/C	[4]
$Zr_{60}Ti_{14.7}Nb_{5.3}Cu_{5.6}Ni_{4.4}Be_{10}$	1200	1850	22.3	650	N/C	[4]
$(Cu_{47}Ti_{33}Zr_{11}Ni_6Sn_2Si_1)_{0.825}(TiB)_{17.5}$	2200	2575	2.0	375	N/C	[5]
$(Mg_{65}Cu_{7.5}Ni_{7.5}Zn_5Ag_5Y_{10})_{0.8}(TiB2)_{20}$	1050	1212	3.2	162	N/C	[6]
$Zr_{48.5}Cu_{46.5}Al_5$	1332	1894	7.7	562	Hardening of crystals	[7]
$Zr_{48.5}Cu_{46.5}Al_5$	1624	1910	6.4	286	Hardening of crystals	[7]
$(Zr_{75}Ti_{18.34}Nb_{6.66})_{0.75}(Be_9Cu_5Ni_4)_{0.25}$	1300	1700	6.0	400	Hardening of crystals	[8]
$Zr_{66.4}Nb_{6.4}Cu_{10.5}Ni_{8.7}Al_8$	1638	1800	1.3	162	Hardening of crystals	[9]
$(Cu_{60}Zr_{30}Ti_{10})_{0.95}Ta_5$	1930	2332	13.3	402	Hardening of crystals	[10]

crystalline phases within the composite samples were monitored independently and analyzed from the kinetic and thermodynamic viewpoints.

2. Experimental procedures

Two different families of the amorphous matrix composites, $Cu_{57}Zr_{28.5}Ti_{9.5}Ta_5$ and $Zr_{56.2}Ti_{13.8}Cu_{6.9}Ni_{5.6}Nb_{5.0}Be_{12.5}$, were used in this study and are hereinafter referred to as samples A and B, respectively. Both samples were cast into a copper mold to produce 40-mm long, 1-mm diameter, cylindrical rods. Samples for compression tests were machined from the cast rods. Uniaxial compression tests were conducted at room temperature on 2-mm long sections under a strain rate of $10^{-4}\,s^{-1}$.

In order to elucidate the hardening behavior during plastic flow, the variations in the cross-sectional area of the sample during compression have to be corrected to display a true stress–strain relation. However, during plastic flow, amorphous alloys with high plasticity do not undergo uniform strain, but rather deform inhomogeneously, leading to a barrel-shaped deformation. Therefore, the conventional conversion procedure, which is used to calculate a true stress by correcting the cross-sectional area of the sample, may lead to an unintentional artifact. As such, the hardness measurement rather than the compression test is considered to be more reliable, because it eliminates the effect of varying geometry of the sample on the strength. For the hardness measurement, the rod samples were machined to a tapered-cylindrical shape such that the cross-sectional area of one end of the rod was larger than the other. This geometry of the test specimens facilitates the occurrence of plastic deformation in a progressive and controlled manner upon compression, thereby enabling the introduction of different strain amounts into the samples. Therefore, the variations in the hardness as a function of plastic strain can be readily traceable by measuring the hardness values at evenly spaced position along the samples' long axis.

The thermal properties of the amorphous composite samples were measured using differential scanning calorimetry (DSC, PerkinElmer DSC7, USA) at a constant heating rate of 30 K/min in a flowing argon atmosphere. The microstructures of the amorphous phases were observed using high resolution transmission electron microscopy (HRTEM, FEI Tecnai G2, field emission gun, 200 kV, The Netherlands). The samples for HRTEM were perforated using electro-chemical thinning in a nital solution (20 vol.% solution of nitric acid in ethanol at $-40\,^{\circ}C$, 40 mA). Since the amorphous phase is prone to be crystallized by the electron beam during TEM observation, all images and patterns were observed and recorded within a few seconds to prevent possible artifacts caused by electron beam-induced crystallization. The shear band propagation behaviors of the deformed samples were observed by scanning electron microscopy (SEM, Nano SEM, FEI, Eindhoven, The Netherlands).

3. Results

Fig. 1 presents the representative microstructures recorded from the two different model alloys A and B. The morphologies and volume fractions of the crystalline particles observed from the two samples were different, revealing different composite microstructures. Sample A contained 10 vol.% of approximately 10-μm diameter, spherical crystalline particles, whereas sample B had 40 vol.% of dendritic crystalline particles with a size greater than 50 μm.
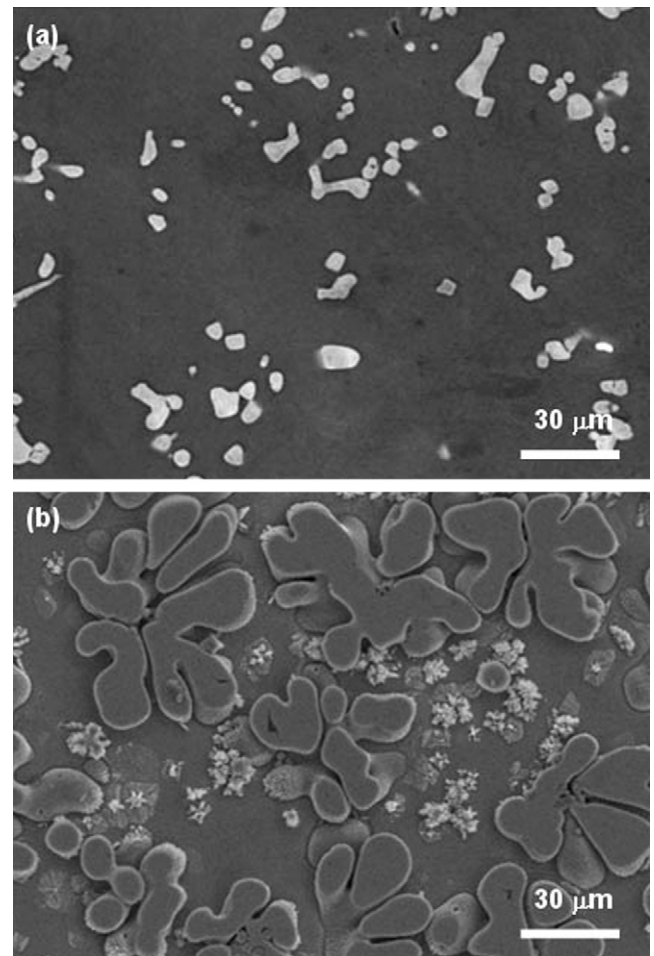

Fig. 1. SEM micrographs of (a) sample A ($Cu_{57}Zr_{28.5}Ti_{9.5}Ta_5$), showing the presence of the Ta-rich crystalline particles with an average size and volume fraction of approximately 10 μm and 10%, respectively and (b) sample B ($Zr_{56.2}Ti_{13.8}Cu_{6.9}Ni_{5.6}Be_{12.5}$), showing dendritic Nb-rich crystalline particles with an average size and volume fraction of approximately 50 μm and 40%, respectively.
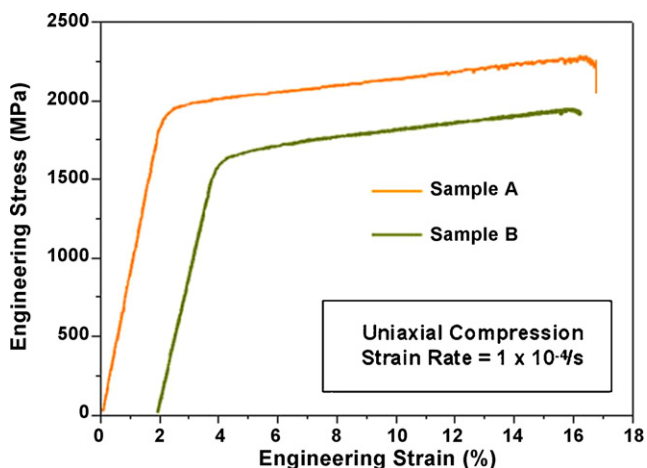
Fig. 2. Uniaxial compressive stress–strain curves measured from samples A and B.

Fig. 2 shows the compressive stress–strain curves corresponding to samples A and B. Sample A showed a yield strength, ultimate strength and fracture strain of 1870 MPa, 2272 MPa and 15.5%, respectively, while those of sample B were 1540 MPa, 1930 MPa and 11%, respectively. It is noteworthy that, during plastic flow, both samples exhibited a strength increment of approximately 400 MPa. However, this strengthening observed from the engineering stress–strain curve is disputable. Therefore, the sample hardnesses were measured directly from the samples subjected to different strains, in order to test if the work hardening is the actual phenomenon that takes place during the plastic flow of amorphous alloys.

Fig. 3 shows the variations in the hardness of the amorphous matrices and the crystalline particles, measured as a function of the strain subjected to samples A and B. The hardness of both amorphous matrices increased linearly with increasing strain, confirming the hardening of the amorphous matrices during plastic flow. However, in the case of the hardness measured from the crystalline particles, different tendencies were observed depending on the particle morphologies. The hardness of the small spherical crystalline particles in sample A did not vary, whereas that of the large dendritic crystalline particles in sample B increased slightly with increasing strain, showing, on the average, a 2.5 VHN increment in the hardness per every 1% increment in the plastic strain. This measured hardness increment is equivalent to a strength increment of approximately 50 MPa, when converted to a strength, under the assumption that the volume fraction of the crystalline particles is approximately 40 vol.%. Since this value is much smaller than the strength increment of approximately 400 MPa observed during plastic flow, the strengthening of the crystalline particles alone is not sufficient to explain the experimentally observed strengthening. Considering the fact that the degree of strengthening is much larger in the amorphous matrices than in the crystalline particles, strengthening of the amorphous matrices, rather than of the crystalline particles, is considered to be the dominant factor affecting the work hardening of the amorphous composites.

4. Discussion

Based on the results of in-situ X-ray scattering, Hufnagel and co-workers [11] claimed that the strengthening of the crystalline particles during compression is responsible for the work hardening of the amorphous matrix composites. In fact, as was observed in the present study, the hardening was observed from the crystalline particles, although its extent varied depending on their morphologies and volume fractions. However, as shown here, the
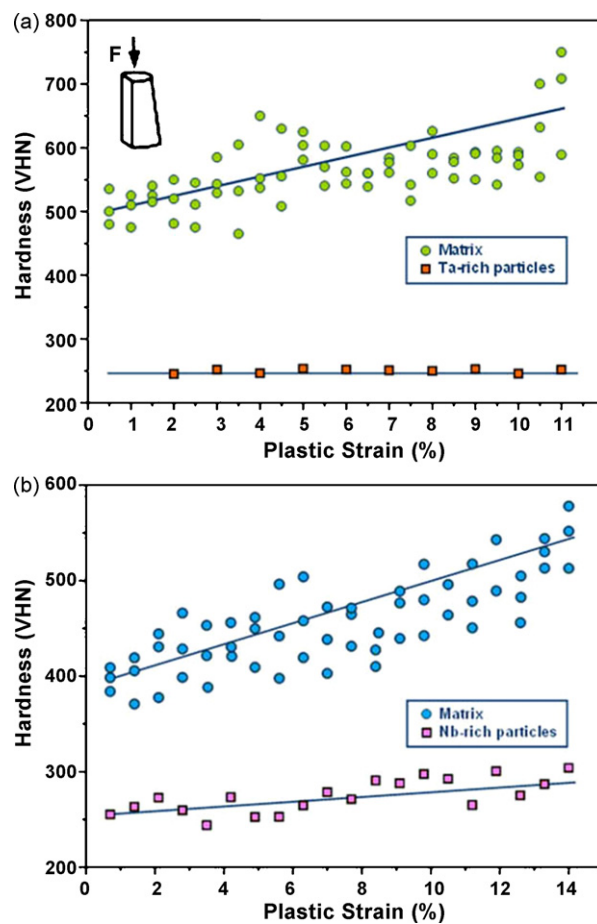

Fig. 3. Variations in the microhardness of the amorphous matrix and crystalline particles measured as a function of the plastic strain imposed on samples (a) A and (b) B.

work hardening of the amorphous composites cannot be explained by the strengthening of the crystalline particles alone. On the other hand, the amorphous matrices exhibited a larger degree of strengthening, regardless of their composition. These experimental findings suggested that the strengthening of the amorphous matrices, rather than of the crystalline particles, is the immediate cause for the work hardening exhibited by the amorphous composites. Therefore, in this section, the origin of the work hardening of the amorphous composites is discussed by separately evaluating the contribution of the constituent phases, i.e., the crystalline particle and amorphous matrix, to the apparent hardening.

4.1. Hardening of crystalline particles

The different hardening behaviors shown by the crystalline phases in Fig. 3 were considered to rely on the different modes of shear band propagation and subsequent interaction with the crystalline particles. Fig. 4(a) presents a micrograph demonstrating the interaction between the propagating shear bands and crystalline particles in sample A. Shear bands were observed to propagate though the interfacial regions between the crystalline particles and amorphous matrix in a tortuous manner, rather than by cutting directly through the particles. This is because it is easier and less energy consuming for the shear bands to propagate along the interfacial regions, due to the low volume fraction, small size and spherical morphology of the crystalline particles. Therefore, in this case, the crystalline particles do not experience shear deforma-
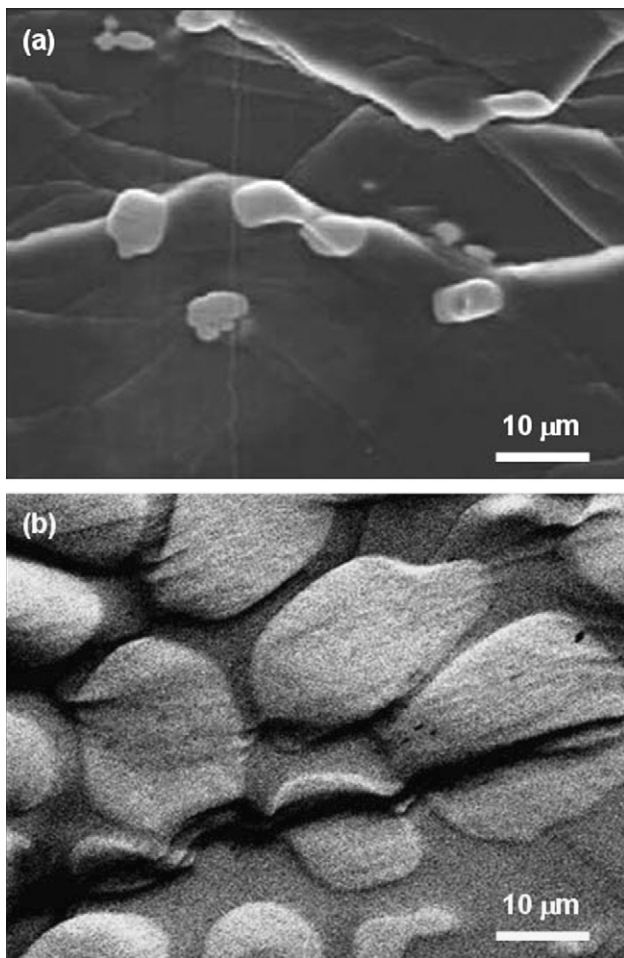
Fig. 4. SEM micrographs showing the different shear band propagation paths observed in samples (a) A and (b) B.

tion and, thus are not hardened, as was confirmed by the hardness measurement in Fig. 3(a).

Unlike sample A, the crystalline particles in sample B were characterized by a dendritic morphology with large volume fraction and size, as shown in Fig. 4(b). These microstructural features facilitated the propagation of shear bands by directly cutting through the narrow dendritic arms, rather than along the winding particle/matrix interfaces in a tortuous manner. As a result, the crystalline particles in sample B experienced shear deformation, causing the particles to be hardened. However, regardless of the strengthening of the crystalline particles, the hardness increment was still much lower in the crystalline particles than in the amorphous matrices. Therefore, the strengthening of the crystalline particles alone was not sufficient to explain the work hardening exhibited by the amorphous composites.

4.2. Hardening of amorphous matrices

In general, the mechanical properties of materials are closely related to their structural changes associated with an externally applied energy (or stress) [16]. Considering that amorphous alloys are not in thermodynamic equilibrium, the application of mechanical energy can induce phase transformation from an amorphous to a more stable crystalline phase. Therefore, in order to understand the origin of the work hardening in the amorphous composites, the microstructures of the amorphous matrices in the as-cast and deformed samples were compared. Since the amorphous matrices of samples A and B both exhibited work hardening, sample B was
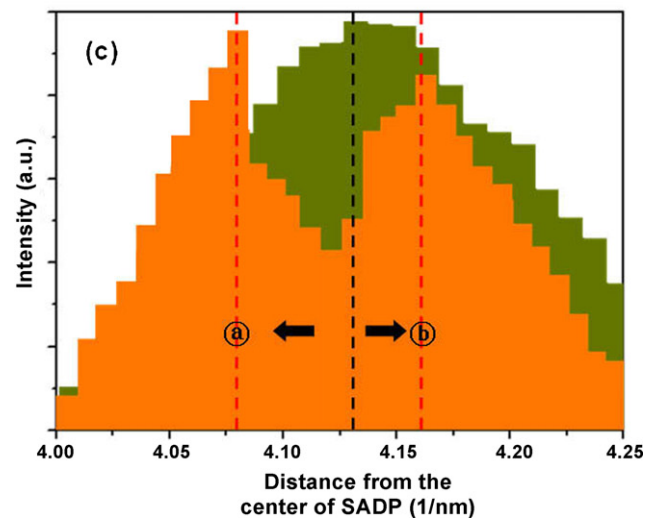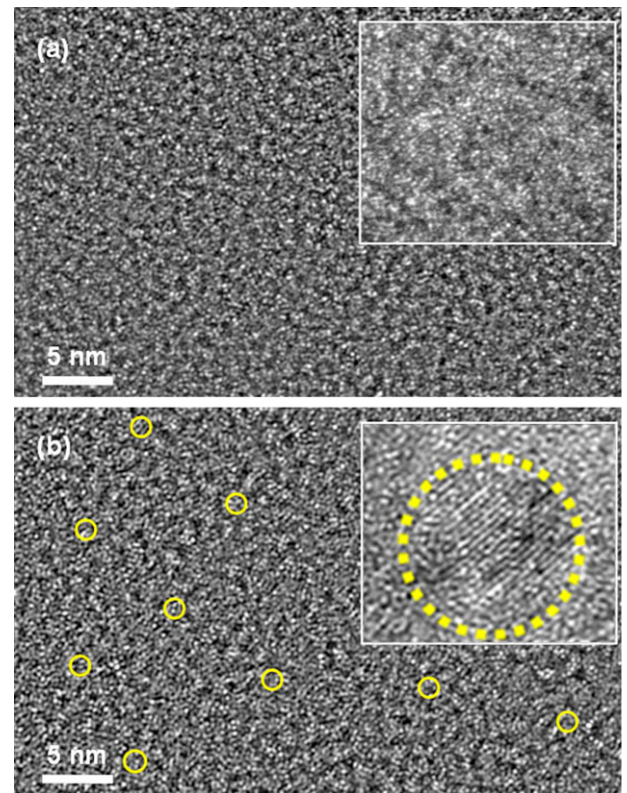

Fig. 5. HRTEM images of (a) the as-cast sample B, showing a fully amorphous structure, and (b) the deformed sample B, exhibiting the presence of nanocrystals with an average size of 1–2 nm embedded in the amorphous matrix. (c) Enlarged view of the SADP intensity profiles obtained from the as-cast sample B (orange), which is superimposed with that of the deformed one (green). (For interpretation of the references to color in this figure legend, the reader is referred to the web version of the article.)

selected as the representative sample to observe the microstructural changes.

Fig. 5(a) shows the HRTEM image of the as-cast sample B, showing a fully amorphous structure without any lattice fringes. However, in the case of the deformed sample, nanocrystals with an average size of 1–2 nm were observed from the amorphous matrix, as shown in Fig. 5(b), suggesting that compression for a prolonged period causes deformation-induced crystallization. Earlier studies on the deformation-induced nanocrystallization in various amorphous alloys supported the result in this study [17–19].

The chemical compositions of the nanocrystals and the remaining amorphous matrix of the deformed sample underwent quantitative analyses using energy dispersive spectroscopy (EDS, data not shown). The nanocrystals exhibited Zr enrichment while the amorphous matrix showed Zr depletion. Similar to sample B, the chemical composition of the nanocrystals in sample A showed Cu enrichment.

The structural differences between the as-cast and deformed samples were further confirmed by comparing the intensity profiles of the selected area diffraction patterns (SADPs). Fig. 5(c) shows the intensity profile of the SADP obtained from the as-cast sample B, which is superimposed with that of the deformed one. The diffraction peak was split into two parts after deformation, indicating that the structural evolution occurred during uniaxial compression. The observed results are readily explained by the earlier interpretation that the shear stress (τ) and hydrostatic pressure (P) associated with uniaxial compression promote the creation of free volume [20] and nanocrystals [10], respectively.

When excess free volume is generated due to shear stress, the average interatomic distance increases, thereby increasing the d-spacing, which, in SADP, appears in a reduced reciprocal lattice distance. Therefore, the left peak (peak (a)) in Fig. 5(c) was considered to have arisen from the creation of excess free volume. On the other hand, when the crystallization occurs by hydrostatic pressure, the average interatomic distance decreases. Therefore, the right peak (peak (b)) was believed to reflect the generation of nanocrystals. In this way, uniaxial compression, which is equivalent to the combined state of shear stress (τ) and hydrostatic pressure (P) at the maximum shear plane, can promote the structural evolution, and crystallization in particular. According to classical nucleation kinetics, the nucleation rate ($\dot{N}$) is expressed as

$$\dot{N} = K \exp\left(-\frac{\Delta G^*}{kT}\right) \exp\left(-\frac{\Delta E_d}{kT}\right),\tag{1}$$

where ΔG^* is the energy barrier for nucleation required to form a critical-sized nucleus, ΔE_d the energy barrier for diffusion required to transport an atom from an amorphous matrix to an embryonic nuclei, and K a constant at a fixed temperature. According to Eq. (1), the nucleation rate can be enhanced if the energy barriers for nucleation (ΔG^*) and diffusion (ΔE_d) are reduced. This section discusses how each stress component influences the values of ΔG^* and ΔE_d, which in turn affect the nanocrystallization process.

4.2.1. Effect of hydrostatic compression on the crystallization

For the homogeneous nucleation of a spherical crystallite with radius r in an amorphous solid, the change in Gibbs free energy associated with the formation of the crystalline nucleus (ΔG) can be expressed as [21]

$$\Delta G(T, P) = \frac{4}{3}\pi r^3 \left(\frac{\Delta G_m + E_e}{V_m^c}\right) + 4\pi r^2 \gamma + P\Delta V,\tag{2}$$

where ΔG_m is the molar free energy change, i.e., the driving force, for an amorphous-to-crystalline phase transformation, E_e the elastic energy induced by a volume change during the phase transformation in the solid state, V_m^c the molar volume of the crystalline phase, γ the interfacial free energy between the crystalline and amorphous phases, and ΔV_m the volume change associated with the formation of a crystalline nucleus. Under the application of hydrostatic pressure (P), the change in the activation energy for nucleation (ΔG^*) is obtained as

$$\left(\frac{\partial(\Delta G^*)}{\partial P}\right)_T = -\frac{64\pi\gamma^3}{3}\frac{\Delta V_m}{(\Delta G_m + E_e + P\Delta V_m)}.\tag{3}$$

The physical meaning of Eq. (3) can be understood by considering the sign of the equation. In the case of the amorphous-to-crystalline transformation, the values for ΔG_m and ΔV_m are both negative and

the elastic strain energy (E_e) associated with this phase transformation is rather low [22]. Therefore, the value of $(\partial(\Delta G^*)/\partial P)_T$ is also negative, indicating that the energy barrier for nucleation required to produce a critical-size nucleus decreases with increasing hydrostatic pressure. Therefore, hydrostatic pressure increases the value of the first exponential term in Eq. (1), thereby enhancing the nucleation rate. This qualitative analysis shows a good agreement with the experimental results reported by Ye and Lu [23], who demonstrated that the application of hydrostatic pressure enhances the precipitation of nanocrystals from the amorphous solid.

4.2.2. Effect of shear stress on the free volume creation

Among two different stress components, shear stress promotes shear-induced atomic dilatation, leading to the generation of free volume, the rate of which ($\dot{v}_f$) can be expressed by Eq. (4) [20]

$$\dot{v}_f = v^* f \exp\left(-\frac{\Delta E_d}{kT}\right) \exp\left(-\frac{\alpha_g v^*}{v_f}\right)$$
$$\times \left[\frac{2\alpha_g kT}{v_f S}\left(\cosh\frac{\tau\Omega}{2kT} - 1\right) - \frac{1}{n_D}\right].\tag{4}$$

This equation describes that the net creation of free volume is determined by the competing role played by the free volume creation rate and the annihilation rate. The model states that the creation rate of free volume becomes larger than the rate of annihilation with increasing shear stress level and under room temperature. This in turn results in atomic dilatation, which enhances the local atomic mobility. From a kinetics perspective, the enhanced atomic mobility should reduce the energy barrier for diffusion (ΔE_d). Therefore, shear stress enhances the value of the second exponential term in Eq. (1), thereby promoting the nucleation of nanocrystals under uniaxial compression.

4.2.3. Crystallinity of the deformed samples

The volume fractions of nanocrystals created during uniaxial compression tests were quantified by measuring the exothermic heat associated with the crystallization. Fig. 6 shows the DSC thermograms obtained from samples A and B in the as-cast and deformed states. Despite the different shapes of the thermograms, the crystallization enthalpies for samples A and B were normally 5–6% smaller in the deformed samples than in the as-cast ones, indicating that the crystallization proceeded by 5–6% during uniaxial compression.

Nanocrystals precipitated during uniaxial compression not only act as the initiation site of shear bands, but also serve as a reinforcing phase. Due to the small size of nanocrystals, neither dislocations nor other types of defects can form or become active within nanocrystals. Therefore, they can be regarded as a perfect crystal having a theoretical shear strength of $\tau \approx G/2\pi$ [24], where G is the shear modulus. Assuming that the shear modulus of Cu and Ti ranges from 37 to 45 GPa [25], and that $\sigma \approx \sqrt{3}\tau$, the normal strength of the Cu-rich and Ti-rich nanocrystals is expected to range within 10–12 GPa. As the normal strength of the Cu- and Ti-based amorphous alloys is 1.6–2.3 GPa, nanocrystals can act as a reinforcing phase. With the experimental values of the volume fraction and strength of the crystalline particles, nanocrystals and amorphous matrices, the strength increments calculated using the phase mixture rule were 400 and 480 MPa for samples A and B, respectively. These values agree reasonably well with the measured increment in strength of approximately 400 MPa. These results strongly support the interpretation presented here that the work hardening of the amorphous composite caused by the deformation-induced nanocrystallization.
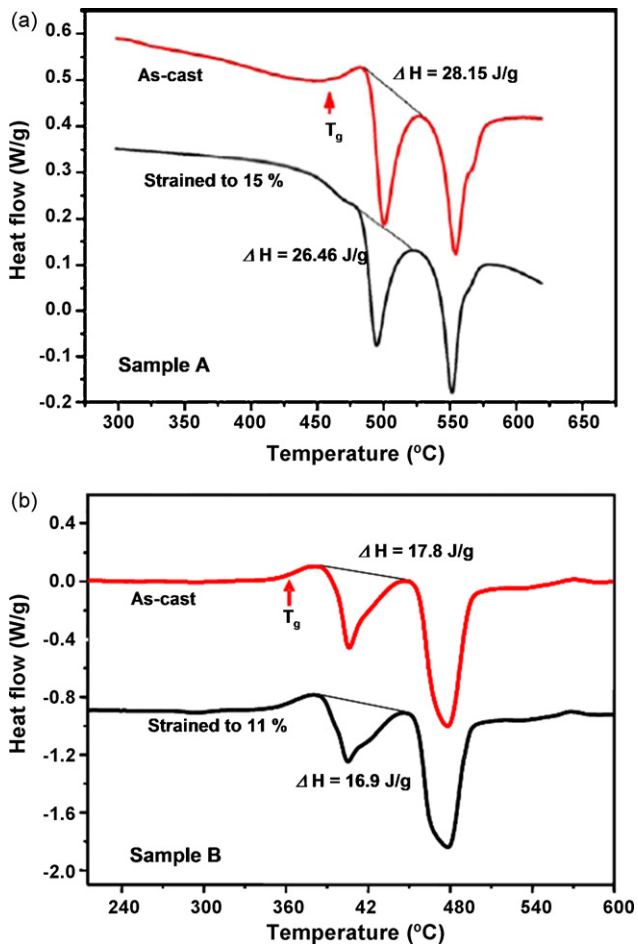
Fig. 6. DSC curves obtained from the as-cast and deformed samples (a) A and (b) B.

hardening of the composites cannot be explained by the work hardening of crystalline particles alone. On the other hand, the amorphous matrices were observed to be hardened due to the formation of nanocrystals precipitated in the amorphous matrices, which supported the work hardening of the amorphous composite. Based on the present experimental results and analysis, the authors propose that deformation-induced crystallization is an important mechanism underlying the hardening of amorphous matrix composites.

References

[1] D.V. Louzguine, H. Kato, A. Inoue, Appl. Phys. Lett. 1088 (2004) 84.
[2] C. Fan, R.T. Ott, T.C. Hufnagel, Appl. Phys. Lett. 1020 (2002) 81.
[3] C. Qin, W.W. Zhang, K. Amiya, K. Asami, A. Inoue, Mater. Sci. Eng. A 230 (2007) 449.
[4] G.Y. Sun, G. Chen, C.T. Liu, G.L. Chen, Scripta Mater. 375 (2006) 55.
[5] H.M. Fu, H. Wang, H.F. Zhang, Z.Q. Hu, Scripta Mater. 1961 (2006) 54.
[6] Y.K. Xu, H. Ma, J. Xu, E. Ma, Acta Mater. 1857 (2005) 53.
[7] Y.F. Sun, B.C. Wei, Y.R. Wang, W.H. Li, T.L. Cheung, C.H. Shek, Appl. Phys. Lett. 051905 (2005) 87.
[8] C.C. Hays, C.P. Kim, W.L. Johnson, Phys. Rev. Lett. 2901 (2000) 84.
[9] U. Kuhn, J. Eckert, N. Mattern, L. Schultz, Appl. Phys. Lett. 2478 (2002) 80.
[10] J.C. Lee, Y.C. Kim, J.P. Ahn, H.S. Kim, Acta Mater. 129 (2005) 53.
[11] R.T. Ott, F. Sansoz, J.F. Molinari, J. Almer, K.T. Ramesh, T.C. Hufnagel, Acta Mater. 1883 (2005) 53.
[12] K.W. Park, J.I. Jang, M. Wakeda, Y. Shibutani, J.C. Lee, Scripta Mater. 805 (2007) 57.
[13] B. Yang, L. Riester, T.G. Nieh, Scripta Mater. 1277 (2006) 54.
[14] J. Eckert, J. Das, K.B. Kim, F. Baier, M.B. Tang, W.H. Wang, Z.F. Zhang, Intermetallics 876 (2006) 14.
[15] R. Bhowmick, R. Raghavan, K. Chattopadhyay, U. Ramamurty, Acta Mater. 4221 (2006) 54.
[16] C.M. Lee, S.C. Lee, S.Y. Shin, N.J. Kim, J.C. Lee, Mater. Sci. Eng. 400 (2008) 487.
[17] H. Chen, Y. He, G.J. Shiflet, S.J. Poon, Nature 541 (1994) 367.
[18] J.J. Kim, Y. Choi, S. Suresh, A.S. Argon, Science 654 (2002) 295.
[19] G.J. Fan, M.X. Quan, Z.Q. Hu, W. Löser, J. Eckert, J. Mater. Res. 3765 (1999) 14.
[20] F. Spaepen, Acta Metall. 407 (1977) 25.
[21] F. Ye, K. Lu, Phys. Rev. B 7018 (1999) 60.
[22] Y.X. Zhuang, J.Z. Jiang, T.J. Zhou, H. Rasmussen, L. Gerward, M. Mezouar, Appl. Phys. Lett. 4133 (2000) 77.
[23] F. Ye, K. Lu, Acta Mater. 2449 (1999) 47.
[24] G.E. Dieter, Mechanical Metallurgy, 3rd ed., McGraw Hill, 1986, p. 119.
[25] J.C. Lee, Y.C. Kim, J.P. Ahn, H.S. Kim, S.H. Lee, B.J. Lee, Acta Mater. 1525 (2004) 52.

5. Conclusion

The present work confirmed the occurrence of work hardening in bulk amorphous composites during quasistatic uniaxial compression. The experimental results suggested that the work